International Journal for Multidisciplinary Research (IJFMR)
E-ISSN: 2582-2160 ● Website: www.ijfmr.com ● Email: editor@ijfmr.com

Eco-Friendly Green Synthesis of Zinc Oxide Nanoparticles from Germinated Finger Millet with Enhanced Antimicrobial and Antioxidant Activities

H.G. Shruthi[1], N.H. Veena[1], B. Pushpa[2], M. Thippeswamy[1*]

[1,*]Department of Studies in Botany, Davangere University, Shivagangotri, Davanagere577002
[2]Department of Chemistry, Davangere University, Shivagangotri, Davangere-577002

[*]**Email: thippeswamym@davangereuniversity.ac.in Mobile No-9480796290**

Abstract

Zinc oxide nanoparticles (ZnO NPs) were synthesized by using germinated finger millet extract which acts as a reducing and stabilizing agent. The synthesized nanoparticles were characterized using XRD, FTIR, UV–visible spectroscopy, SEM–EDX, TEM, and DLS analyses. XRD confirmed the crystalline nature of ZnO with an average crystallite size of approximately 28 nm, while UV–visible spectroscopy displayed a characteristic absorption peak at 368 nm. SEM and TEM analyses revealed predominantly spherical nanoparticles with noticeable agglomeration, and EDX analysis confirmed the presence of zinc and oxygen elements. The synthesized ZnO nanoparticles were evaluated for antimicrobial and antioxidant assays. The nanoparticles exhibited significant antifungal action against Aspergillus flavus and Pichia anomala, as well as antibacterial activity against Staphylococcus aureus, Enterococcus faecalis, Escherichia coli, and Pseudomonas aeruginosa. Furthermore, the nanoparticles showed a DPPH radical scavenging IC^{21} value of 104.23 µg/mL, indicating a moderate antioxidant activity. These findings indicate that the green-synthesized ZnO nanoparticles possess promising biological applications.

Keywords: Antimicrobial activities, Germinated Eleusine coracana,Finger millet, Nanoparticles, Zinc oxide,

Graphical abstract

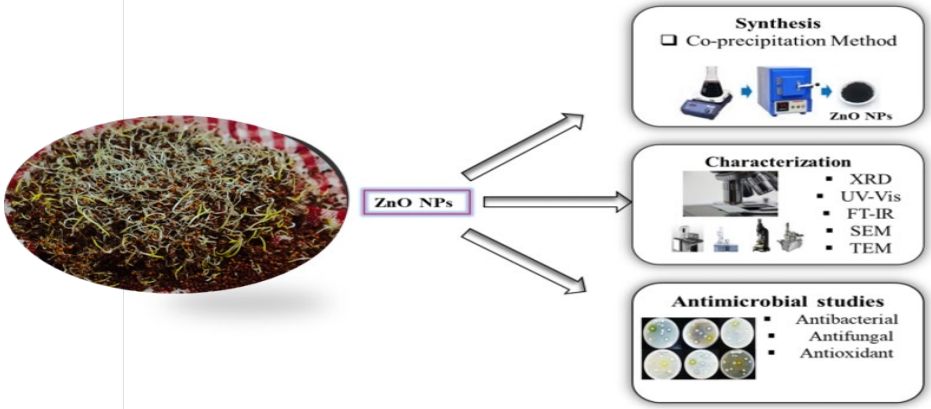

1. Introduction

Green synthesis has emerged as a promising and sustainable strategy for nanoparticle production, providing a number of benefits over traditional conventional physical and chemical synthesis methods. This approach is cost-effective, environmentally benign, and easily scalable for large-scale manufacturing [1]. Moreover, green synthesis avoids the use of high temperatures, elevated pressures, excessive energy input, and toxic chemical reagents, thereby minimizing environmental and health-related concerns [2]. Among the various biological resources available, plant extracts are the most widely employed owing to their abundance, accessibility, and lower toxicity compared to microbial systems. A wide variety of bioactive substances, like polyphenols, polysaccharides, amino acids, vitamins, alkaloids, and other secondary metabolites, are present in these extracts and serve as reducing, stabilizing, and capping agents during the creation of nanoparticles [3, 4].

Among nanoparticles made of metal oxides, Zinc oxide nanoparticles, or ZnO NPs, have garnered a lot of interest because of their distinct physicochemical characteristics and wide variety of uses in fields like biology, chemistry, medicine, and physics [5–8]. More recently, their potential utility in agriculture has also gained more recognition [9, 10]. Zinc oxide is an inexpensive inorganic material that is generally regarded as safe and non-toxic by the Food and Drug Administration (FDA). Several studies have shown that by enhancing nutrient uptake, seed germination, and physiological performance, ZnO NPs can improve plant growth, development, and production when applied at the right concentrations. [11, 12].

In recent times, zinc oxide NPs received substantial interest for their distinctive physicochemical attributes, which include a high surface area, chemical stability, biocompatibility and unique optical and antimicrobial properties. These properties transform ZnO nanoparticles highly suited for an extensive range of applications in the therapeutic, ecological and catalytic sectors. Traditionally, ZnO NPs are prepared through physical and chemical methods; despite this, these methods frequently necessitate the use of toxic reactants, high energy usage and environmental issues [1-3]. For this reason, nanotechnology research has prioritized the emergence of sustainable and globally acceptable synthesis methodologies [4]. The extensive use of plant extracts in the green synthesis of nanoparticles has been recognized as a comparatively inexpensive, environmentally friendly and efficient replacement. During the growth of nanoparticles, plant-based synthesis employs naturally derived phytochemicals, including phenolics, flavonoids, proteins and carbohydrates which serve as both stabilizing and reducing agents. In spite of their superior biochemical composition and biological activities in comparison to their germination-free counterparts, germinated cereals are receiving an increasing amount of prominence among a variety of plant sources [5-7]. Finger millet (Eleusine coracana), a cereal that is abundantly

cultivated in numerous regions of the globe and is noteworthy for its high concentration of antioxidants, trace elements, dietary fibers and phyto-nutrients. Germination further improves its the phytochemical profile, which enhances its effectiveness as a biological-reducing agent in the creation of nanoparticles [8, 9]. The implementation of germinated finger millet extract in the synthesis of nanoparticles is comparatively limited regardless its nutritious and therapeutic importance.

S. Abdelbaky et al. synthesized spherical ZnO nanoparticles using Cymbopogon citratus leaf extract, exhibiting a characteristic absorption peak at 370 nm and high antioxidant activity, as evidenced by the 45.67 ± 0.1 µg/mL IC•₀ value. The biosynthesized ZnO NPs also demonstrated strong anti-inflammatory activity at 1 mg/mL of 98.1 ± 0.04% as opposed to 92.1 ± 0.07% for indomethacin, along with significant antimicrobial and selective antitumor properties against a range of human cancer cell lines [10]. T. S. Aldeen et. al reported a green synthesis method for ZnO nanoparticles using Phoenix roebelenii palm as a natural chelating agent, stabilizing agent. The synthesized ZnO nanoparticles demonstrated strong antibacterial efficacy against gram-negative (Escherichia coli and Salmonella typhi) and gram-positive (Staphylococcus aureus and Streptococcus pneumoniae) bacterial strains [11]. A. K. Pillai et al. reported the quick and environmentally friendly green synthesis of ZnO nanoparticles utilizing extracts of Beta vulgaris, Cinnamomum tamala, Cinnamomum verum, and Brassica oleracea var. italica.The produced ZnO nanoparticles had strong antifungal activity against Candida albicans and Aspergillus niger as well as antibacterial activity against Escherichia coli and Staphylococcus aureus, suggesting their potential as potent antimicrobial agents [12].

In this research, ZnO nanoparticles were synthesized through a green synthesis approach using germinated Eleusine coracana extract. The produced nanoparticles were described by XRD, FTIR, UV–vis, SEM–EDX, TEM, and DLS analyses. Furthermore, the produced ZnO nanoparticles were investigated for their biological activities, including antimicrobial and antioxidant properties.

Sr. No	Plants/plant extracts	Nanoparticle size	Shape	Application	Reference
1	Dry ginger rhizome	23-26 nm	spherical in shape	Antimicrobial activity	[13]
2	Cassia fistula	5–15 nm	Sponge like irregular shape	Antioxidant activity	[14]
3	Vaccinium arctostaphylosL	-	Spherical in shape	Antidiabetic activity	[15]
4	C. citratus ALE	21 nm	Spherical in shape	Antioxidant, anti-inflammatory, anti-microbial, and cytotoxic potencies	[16]
5.	Trifolium pratense flower extract	Below 100 to 190 nm	Agglomerated	Antibacterial activity	[17]
6	chamomile flower (Matricaria chamomilla L.), olive	40.5 to 124.0 nm	-	Antibacterial	[18]

	leave (Olea europaea) and red tomato fruit (Lycopersicon esculentum M.)				
7	Punica granatum fruit peels	32.98 nm and 81.84 nm	Spherical and hexagonal-shape	Antibacterial activities and cytotoxicity	[19]
8	S. nigrum leaf extract	20 and 30 nm	Quasi-spherical in shape	Antibacterial	[20]
9	Pongamia pinnata plant extract	100 nm	Spherical nature	Antibacterial	[21]
10	Vitex negundo plant extract	75 to 80 nm	Spherical	Antibacterial activity	[22]

2.0. Materials and methods

2.1 Material:

Finger millet seeds were collected by farmers of jagalur taluk, davangere district, and zinc nitrate hexahydrate [$Zn(NO_3)_2.6H_2O$] is purchased by vikas scientific, sdfine chemicals. Since all of the reagents are analytical grade, no additional purification is required.

2.2. Synthesis of ZnO NPs

20 g of finger millet seeds (Eleusine coracana) were immersed in distilled water for 24 hrs at room temperature to facilitate hydration. After that the soaked seeds were drained and allowed to germinate. On the fifth day of germination, the sprouts were carefully cleaned using distilled water and homogenized by using a mortar and pestle to obtain a uniform paste. The resulting paste was dispersed in distilled water (100 mL) in a in a 250 mL beaker and stirred for 1hr maintaining temperature 75^0Cat 450–600 rpm. Whatman No. 1 filter paper was utilized for filter the mixture once it had naturally cooled to room temperature. The clear filtrate was collected and preserved for subsequent use in the environmentally friendly production of zinc oxide nanoparticles [23, 24].

3 g of zinc nitrate hexahydrate [$Zn(NO_3)_2.6H_2O$] was dissolved in 40 mL of distilled water. Then 10 mL of the aqueous Finger millet extract were added drop by drop. The reaction mixture was stirred well and filtered. Then the ZnO NPs were calcined in a muffle furnace at 450 °C for 3 hrs [25].

2.3 Characterization

To investigate the crystalline structure and size of the ZnO, XRD analysis was carried out employing a Bruker D8 Advance powder diffractometer. Chemical functional groups were found using FTIR spectroscopy (JASCO 6800) across the 400–4000 cm^{-1} range, while UV-Vis spectroscopy (DS5Graphic_RGB-1024x667) was utilized to examine absorption characteristics. Morphological features and composition of elements were determined using SEM and EDX (Neo-Scope JCM-6000 PLUS), with Transmission electron microscopy (TEM) analysis was carried out with a JEOL JEM-2100 device to study the particle size and morphology. The hydrodynamic size distribution of the produced ZnO NPs was evaluated using DLS.

2.4 Antimicrobial Activity by Agar Well Diffusion Method

The agar well diffusion method was empolyed to evaluate the generated samples' antibacterial activity

investigated by Ranjitha et al. with slight modifications [26, 27]. Gram-positive bacterial strains, such as Staphylococcus aureus (ATCC-737) and Enterococcus faecalis (ATCC-51299), as well as Gram-negative bacterial strains, such as Pseudomonas aeruginosa (ATCC-15442) and Escherichia coli (ATCC-443), were used to test the antibacterial potential. Sterile saline solution was used to adjust the inoculum density to roughly 5×10^1 CFU/mL. The DMSO was used to dissolve the samples to prepare a stock solution of 20 mg/mL, and different concentrations were introduced into the wells of the agar plates. Luria–Bertani agar medium was used for bacterial cultures, whereas Potato–Dextrose agar medium was employed for fungal strains. For bacterial cultures, the plates were incubated at 37 °C, while for fungal cultures, they were incubated at 28 °C for 72 hours. The diameter of the inhibitory zones was measured in millimeters (mm) to ascertain the level of antibacterial activity.

2.5 DPPH Free Radical Scavenging Assay

The DPPH (2,2-diphenyl-1-picrylhydrazyl) assay for free radical scavenging was utilized to measure the materials' antioxidant activity, according to the method described by Blois (1958). Briefly, various concentrations of the sample were mixed with 2 mL of DPPH solution (100 µM) and the total volume was adjusted to 3 mL using methanol. For forty-five minutes, the reaction mixture was allowed to sit at room temperature in the dark. Following incubation, A UV-Vis spectrophotometer (Shimadzu UV-1800, Kyoto, Japan) was employed to identify the absorbance at 517 nm with a blank solution (without sample/standard) as reference.Butylated hydroxytoluene (BHT) served as the antioxidant reference to calculate and express the radical scavenging activity as $IC_{\cdot}{}^{1}$ values.

2.6 Ferrous Ion Chelating Assay

The ferrous ion chelating activity of the samples was evaluated using the approach reported by Danis et al. with slight modifications [28]. Briefly, different concentrations of each sample that had been suitably diluted was combined with 0.05 mL of a 2 mM $FeCl_2$ solution. 0.1 mL of a 5 mM ferrozine solution was included to start the reaction, and it was left to rest at room temperature for ten minutes. Following incubation, a spectrophotometer was employed to measure the absorbance of the colored complex at 562 nm in comparison to a blank solution made without a sample or standard. Afterwards, the % suppression of ferrozine–Fe2 compound formation was computed and the chelating activity was expressed as IC_{50} values using Ethylenediaminetetraacetic acid (EDTA) as the reference standard.

3.0. Results and Discussion

3.1 X-ray diffraction analysis (XRD)

The produced ZnO NPs' XRD patterns are depicted in Fig. 1. The XRD analysis of ZnO NPs reveals prominent diffraction maximums at 2θ values of 31.8°, 34.5°, 36.5°, 47.7°, 56.6°, 63.0°, 66.46°, 68.1°, 69.2°, 72.8°, and 77.2°, which correspond to the (001), (200), (101), (201), (110), (301), (002), (211), (102), (400) and (202) crystallographic planes, respectively. The development of the ZnO's hexagonal wurtzite structure is confirmed by these diffraction features, which closely match the typical ZnO pattern published in JCPDS card No. 79-0205. [29].

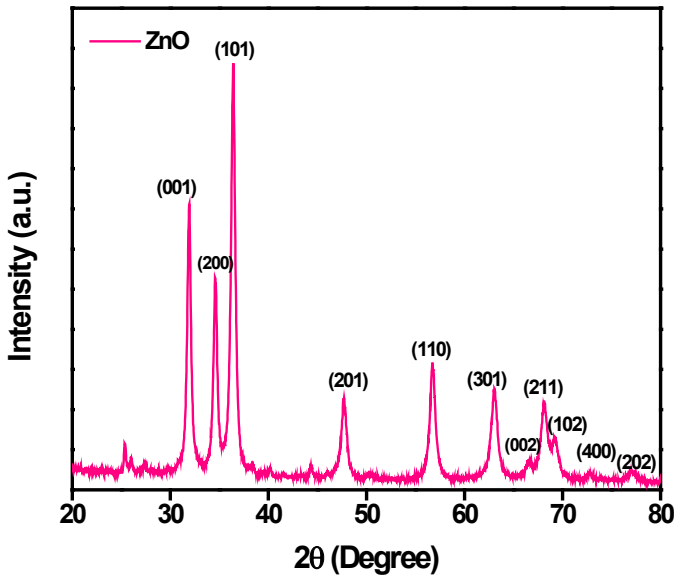

Figure. 1: **XRD pattern of synthesized ZnO nanoparticles**

The Debye–Scherrer equation (Equation 1) was employed to determine the average crystallite size of the synthesized samples, according to the strongest diffraction peaks' full width at half maximum (FWHM).

$$D = \frac{k\lambda}{\beta \cos \theta} \text{----------(1)}$$

D stands for crystallite size, k for form factor (0.90), λ for the CuKα line (1.54 Å), "Full width at Half Maxima," and θ for the matching angle. ZnO NPs had an average crystallite size of 28 nm.

3.2 Fourier transform infrared spectroscopy

The FTIR spectrum of ZnO nanoparticles produced using finger millet extract showed a broad band at 3416 cm^{-1} corresponding to O–H stretching of hydroxyl groups and adsorbed water. The peaks at 2928 cm^{-1} and 2855 cm^{-1} are attributed to aliphatic C–H stretching vibrations. Bands at 1742 cm^{-1}, 1618 cm^{-1}, and 1524 cm^{-1} arise from carbonyl (C=O), aromatic C=C, and amide-related functional groups of phytochemicals. The peaks at 1451 cm^{-1}, 1378 cm^{-1}, 1254 cm^{-1}, 1160 cm^{-1}, and 1098 cm^{-1} correspond to C–H bending and C–O stretching vibrations of phenolic and carbohydrate constituents. The characteristic band at 566 cm^{-1} is attributed to Zn–O stretching, verifying ZnO nanoparticle production. The presence of these biomolecular functional groups suggests their function in ZnO nanoparticle stability and decrease [30].

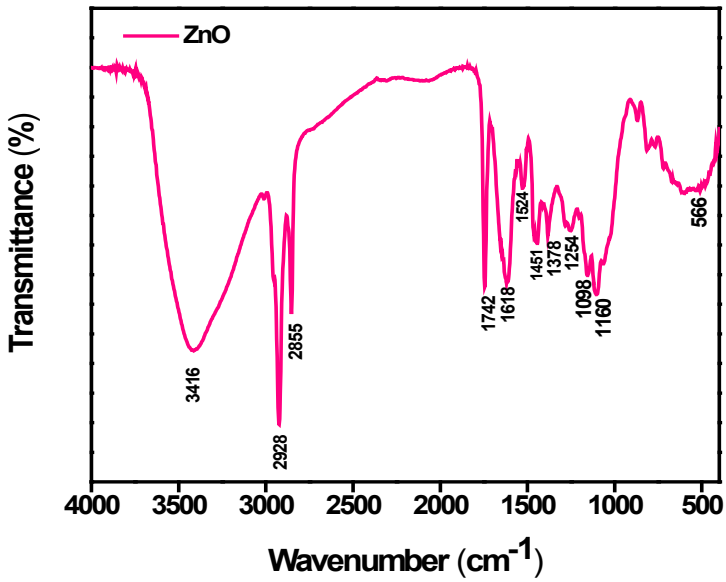

Figure. 2: **FTIR Spectra of synthesized ZnO NPs**

3.3 UV-vis spectroscopy

The UV-Visible absorption spectrum of the produced ZnO NPs is depicted in Fig. 3a. A strong absorption peak is observed at around 368 nm, which is characteristic of ZnO and corresponds to its intrinsic band edge absorption. Tauc's approach was employed to gauge the ZnO NPs' optical band gap energy (Eg) [30]. As seen in Fig. 3b, the Tauc plot was created by graphing (αhv)2 against photon energy (hυ).

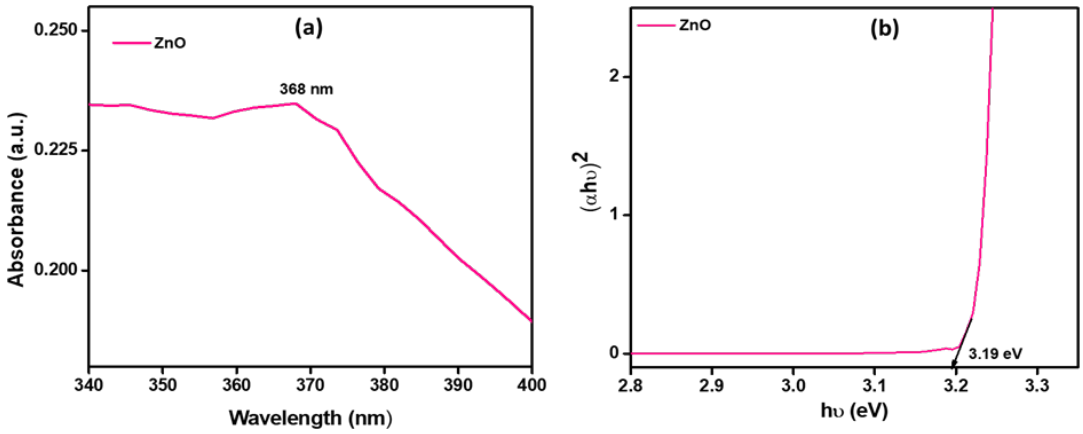

Figure. 3: **(a) UV-Vis diffused absorbance spectrum and (b) Energy band gap of ZnO NPs**

The band gap was determined by extending the linear part of the plot to the energy axis, following Equation (2).

$\alpha hv = A[hv - E_g]^{n}$,..... (2)

where the band gap energy is Eg, the photon energy is hv, index n varies depending on the kind of electronic transitions, the absorption coefficient is α, and the absorption constants for indirect transitions are A. Direct-allowed optical transitions have n values of 1/2, while indirect-allowed optical transitions have n values of 2. The energy band gap value was calculated by extending the curve's linear component to the x-axis [31]. The ZnO NPs' computed optical band gap energy (Eg) was determined to be roughly 3.19 eV.

3.4. Scanning Electron Microscopy combined with Energy Dispersive X-ray (EDX)

The elemental composition and surface morphology of the produced ZnO NPs were examined using Energy Dispersive X-ray (EDX) spectroscopy in conjunction with Scanning Electron Microscopy (SEM). SEM pictures of ZnO NPs at various magnifications are shown in Fig. 4(a–d), revealing the formation of irregularly shaped clusters composed of spherical grains. The nanoparticles exhibit a porous surface structure with evident agglomeration, resulting in a heterostructured morphology [32, 33]. Such morphological features are known to enhance surface area and provide more active sites, which are advantageous for various catalytic and sensing applications. The corresponding EDX spectrum, depicted in Fig. 4(e), confirms the effective synthesis of ZnO NPs within the composite by confirming the elemental composition of the sample, revealing the presence of zinc (Zn) and oxygen (O).

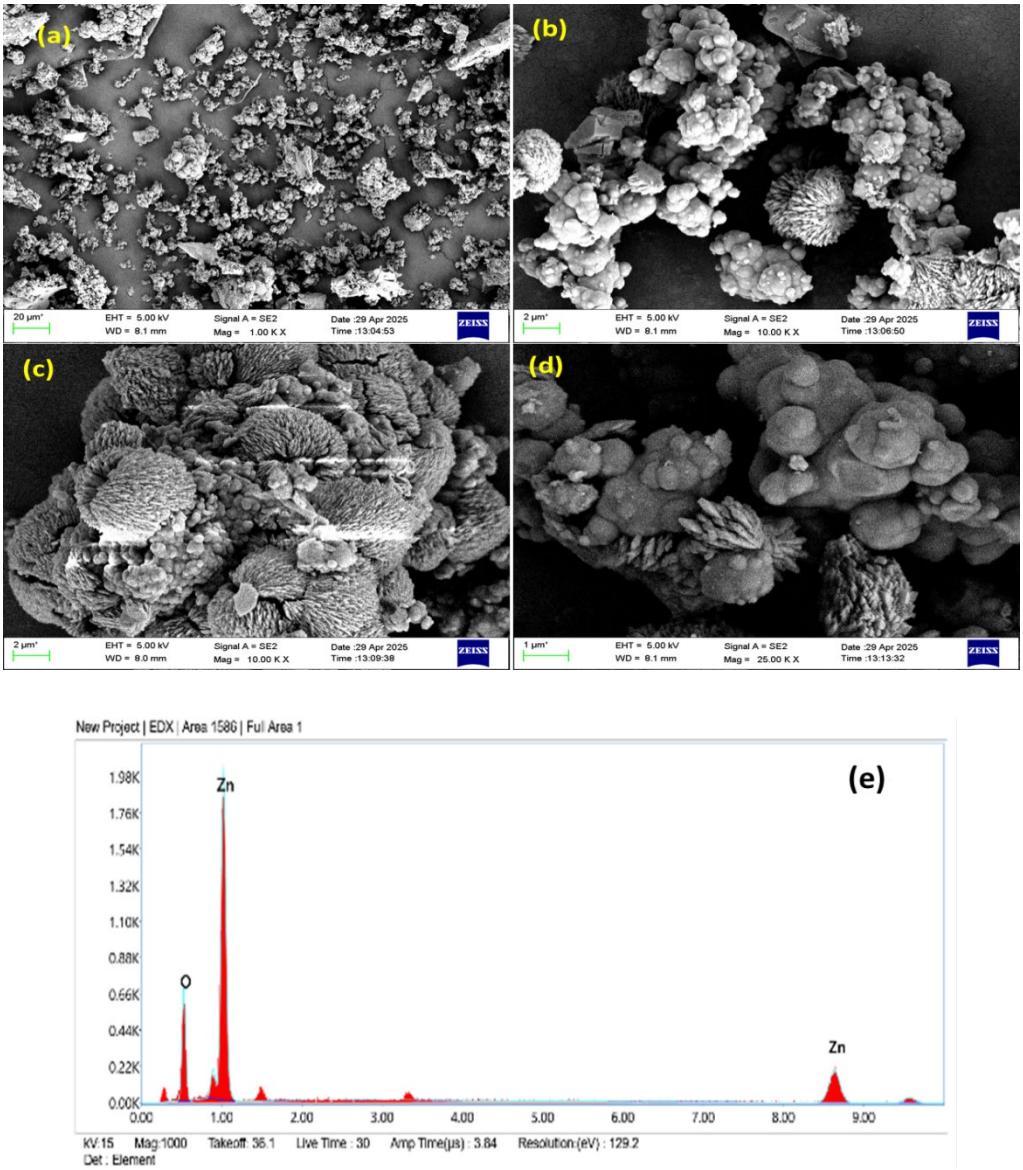

Figure. 4. (a-d) SEM images of synthesized ZnO NPs at different magnification and (e) EDX spectra of ZnO NPs.

3.5 Transmission Electron Microscopy (TEM)

Fig. 5(a-d) presents the TEM analysis of the synthesized ZnO NPs, revealing clear morphological and structural characteristics. The nanoparticles display predominantly spherical coral like shapes with noticeable agglomeration, probably as a result of strong interparticle interactions. A broad size distribution is observed, indicative of nanoscale aggregation. High-resolution TEM (HRTEM) images display distinct lattice fringes, confirming their crystalline nature, in accordance with XRD results. The measured interplanar spacing of 0.28 nm corresponds to the (001) plane of ZnO. The SAED pattern shows diffuse rings, characteristic of a polycrystalline structure, with d-spacings matching well with the (200) planes identified in XRD analysis [34].

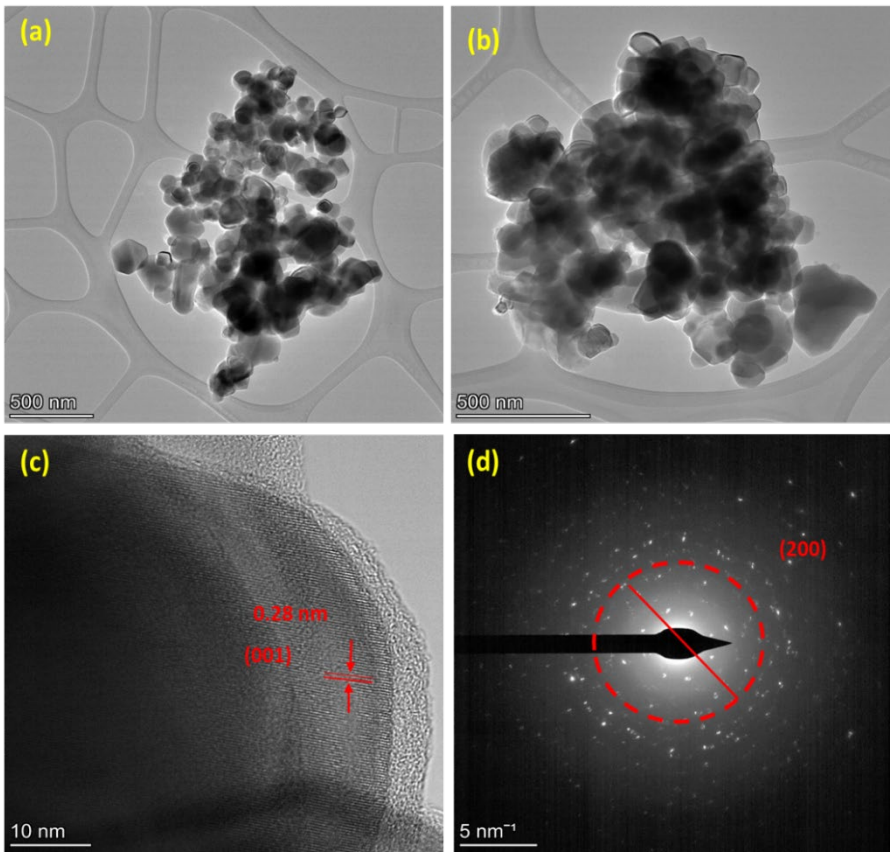

Figure. 5. (a-b) TEM images of synthesized ZnO NPs (c) HRTEM and (d) SEAD pattern spectra of ZnO NPs.

3.6 Dynamic Light Scattering (DLS)

The hydrodynamic size distribution of the generated ZnO NPs was assessed using the Dynamic Light Scattering (DLS) technique. As demonstrated in Fig. 6, the DLS spectrum indicates a relatively narrow and consistent size distribution, with a typical particle diameter of approximately107.3 nm [35, 36].

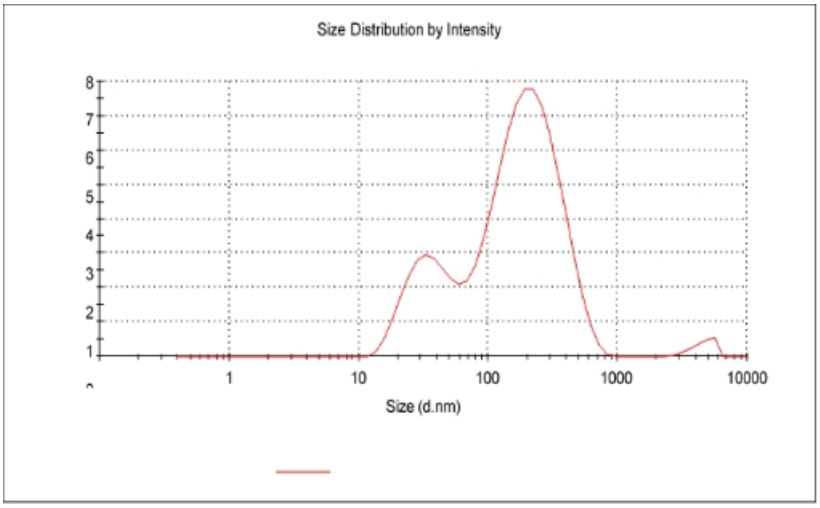

Figure.6:DLS spectra of synthesizes ZnO NPs

3.7 Pharmacological activities

ZnO NPs that were synthesized were used to assess the radical scavenging ability of the extracts and their resistance to a variety of pathogens. To find inhibition zones and MICs, extracts aretested against both Gram-negative (Escherichia coli) and Gram-positive (Staphylococcus aureus) germs. To check whether the extract inhibits mycelial growth or spore germination, Candida albicans and Aspergillus niger are assayed.Most radical scavenging tests use the DPPH (2,2-diphenyl-1-picrylhydrazyl) technique to determine the free radical neutralization of the extract. An elevated phenolic content is frequently a type of antioxidant.Sickle cell disease (SCD) and other uncommon anemias needing continuous blood transfusions require iron chelation. Prevention of iron overload is the main goal of iron chelation treatment [37, 38].

3.8 Antibacterial activity

The produced ZnO nanoparticles' (ZnO NPs) antimicrobial activity was systematically investigated against both Gram-positive and Gram-negative bacterial pathogens using the agar well diffusion method, and the obtained results are summarized in Table 1 and illustrated in Fig. 7. The tested Gram-positive bacterial strains included Staphylococcus aureus (ATCC-737) and Enterococcus faecalis (ATCC-51299), while the Gram-negative strains comprised Escherichia coli (ATCC-443) and Pseudomonas aeruginosa (ATCC-15442). The produced ZnO NPs exhibited a clear concentration-dependent antibacterial activity, where no measurable inhibition zones were observed for the blank, 100 µg, and 200 µg concentrations, indicating negligible antimicrobial efficacy at lower concentrations. However, appreciable antibacterial activity was detected at concentrations of 300 and 400 µg. At 300 µg, the ZnO NPs produced inhibition zone diameters of 7.66 ± 1.15 mm against Staphylococcus aureus, 8.66 ± 0.57 mm against Escherichia coli, 8.33 ± 0.57 mm against Enterococcus faecalis, and 10.33 ± 1.15 mm against Pseudomonas aeruginosa. A further increase in nanoparticle concentration to 400 µg significantly enhanced the antibacterial performance, yielding inhibition zones of 14.66 ± 0.57 mm, 11.66 ± 1.15 mm, 13.33 ± 0.57 mm, and 11.33 ± 1.15 mm against Staphylococcus aureus, Escherichia coli, Enterococcusfaecalis, and Pseudomonas aeruginosa, respectively. Among all the tested bacterial strains, Staphylococcus aureus exhibited the highest susceptibility toward ZnO NPs, followed by Enterococcus faecalis, whereas comparatively there was a moderate level of antibacterial activity against the Gram-negative strains. The superior antibacterial efficacy of ZnO NPs could be ascribed to their nanoscale dimensions and high surface area, which facilitate strong interactions with bacterial cell membranes. Furthermore, oxidative

stress can be caused by the Zn2+ ion release, the generation of reactive oxygen species (ROS), and the consequent loss of membrane integrity, leakage of intracellular components, and eventual bacterial cell death. These results unequivocally show that the produced ZnO nanoparticles have substantial broad-spectrum antibacterial potential and could be used as potential antibacterial agents for use in medicine and biomedicine.

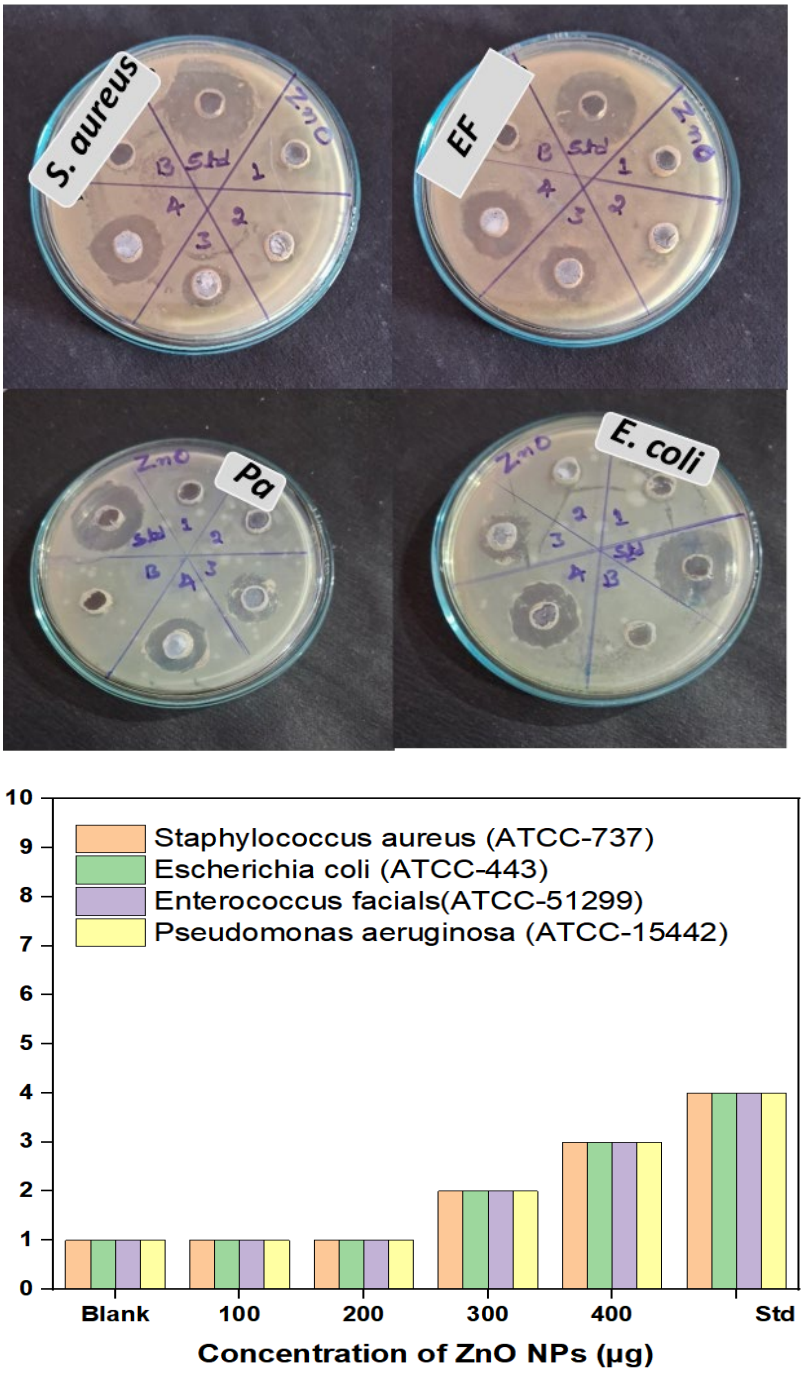

Figure.7. Antibacterial activity of ZnO NPs against bacterial strains such as (a) Escherichia coli (b) Staphylococcus aureus, (b)E. faecalis, (c) Pseudomonas aeruginosa and Agar well diffusion method (e) Bargraph antibactirial activity of ZnO NPs.

Table-1 : The antibacterial activity shown by the ZnO NPs towards different gram- positive and gram-negative bacterial samples

Sl.No	Sample Name	Conc. (µg)	S. aureus	E. coli	E.faecalis	P.aeruginosa
1	ZnO	Blank	---	---	---	---
		100	---	---	---	---
		200	---	---	---	---
		300	7.66 ± 1.15	8.66 ± 0.57	8.33 ± 0.57	10.33 ± 1.15
		400	14.66 ± 0.57	11.66 ± 1.15	13.33 ± 0.57	11.33 ± 1.15

3.9 Antifungal activity

Using the agar well diffusion method, the antifungal activity of the produced ZnO nanoparticles (ZnO NPs) was assessed against Aspergillus flavus and Pichia anamola. The results are summarized in Table 2 and shown in Fig. 8. The ZnO NPs exhibited significant concentration-dependent antifungal activity against both fungal pathogens. No inhibition zone was observed for the blank sample, while minimal antifungal activity was detected at lower concentrations. At 100 µg concentration, no inhibition was observed against Aspergillus flavus, whereas an inhibition zone of 7.33 ± 0.57 mm was recorded against Pichia anamola. Upon increasing the concentration to 200 µg, the inhibition zones increased to 8.66 ± 0.57 mm and 9.66 ± 0.57 mm against Aspergillus flavus and Pichia anamola, respectively. Further enhancement in antifungal efficacy was observed at 300 µg, where both fungal strains exhibited inhibition zones of 11.66 ± 0.57 mm. The highest level of antifungal activity was attained at 400 µg, with inhibition zone diameters of 15.66 ± 0.57 mm against Aspergillus flavus and 17.33 ± 0.57 mm against Pichia anamola, which were similar to the typical medication values of 15.33 ± 0.57 mm and 16.33 ± 0.57 mm, respectively. Among the tested fungal strains, Pichia anamola exhibited relatively higher susceptibility toward ZnO NPs. The enhanced antifungal activity of ZnO NPs could be linked to the production of reactive oxygen species (ROS), disruption of fungal cell membrane integrity, and interaction of Zn^{2+} ions with intracellular biomolecules, ultimately resulting in fungal cell damage and growth inhibition. These findings demonstrate that the synthesized ZnO nanoparticles possess promising antifungal potential against pathogenic fungal species.

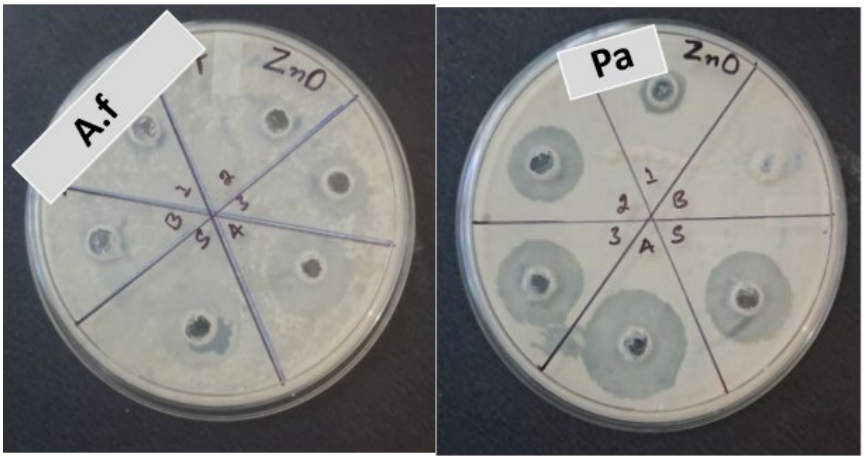

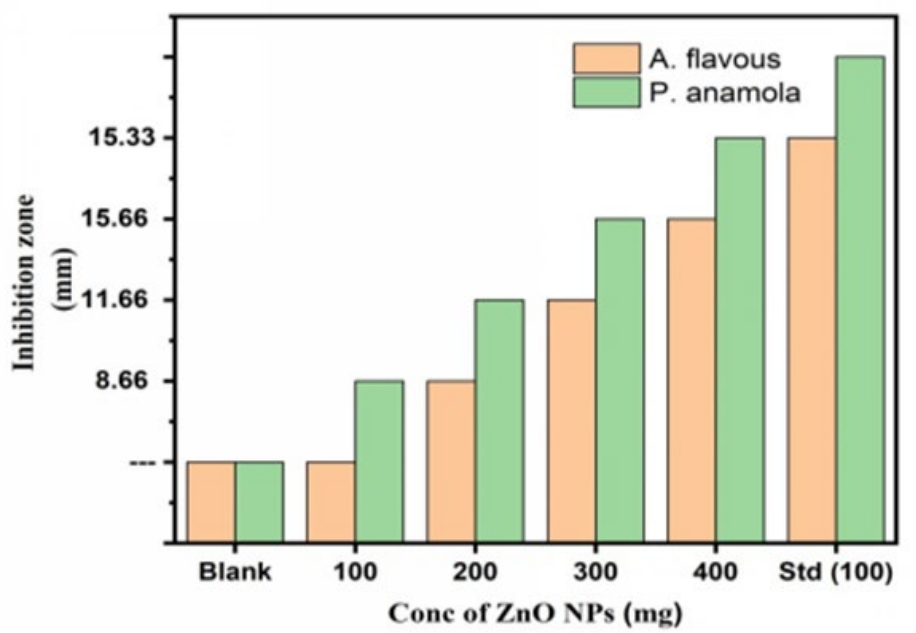

Figure.8.Anti-fungal activity of ZnO NPs against fungal strains such (a) Aspergillus flavus and (b)Pichia anomala (c) Bargraph antifungal activity of ZnO NPs.

Table-2 : The antifungal activity shown by the ZnO NPs towards different fungal samples

Sl.No	Sample Name	Conc. (µg)	A. flavous	P. anamola
1	ZnO	Blank	---	---
		100	---	7.33 ± 0.57
		200	8.66 ± 0.57	9.66 ± 0.57
		300	11.66 ± 0.57	11.66 ± 0.57
		400	15.66 ± 0.57	17.33 ± 0.57
		Std (100)	15.33± 0.57	16.33± 0.57

3.10 Antioxidant activity by DPPH method

The antioxidant characteristics of the produced ZnO nanoparticles (ZnO NPs) were investigated by scavenging free radicals with DPPH and ferrous-ion chelation assays, and the obtained IC_{50} values are presented in Table 3 and Fig. 9–10. In the DPPH assay, ZnO NPs demonstrated moderate radical scavenging efficiency with an IC_{50} value of 104.23 µg/mL, compared to the standard antioxidant Vitamin C, which showed a lower IC_{50} value of 23.59 µg/mL. However, in the ferrous-ion chelation study, the ZnO NPs exhibited very weak chelating performance, and no measurable IC_{50} value was achieved within the tested concentration range, whereas EDTA displayed an IC_{50} value of 44.66 µg/mL. These observations indicate that the antioxidant behavior of ZnO NPs is mainly attributed to their capacity to scavenge free radicals rather than their metal ion chelating potential.

Table-3 : Results obtained from DPPH IC_{50} and Ferrous-Ion Chelation analysis for ZnO NPs in comparision with the standard sample.

Sl No	Samples	DPPH IC_{50} (µg/mL)	Ferrous-Ion Chelating IC_{50} (µg/mL)
1	ZnO	104.23	No Activity
2	Std	23.596 (Vit-C)	44.66 (EDTA)

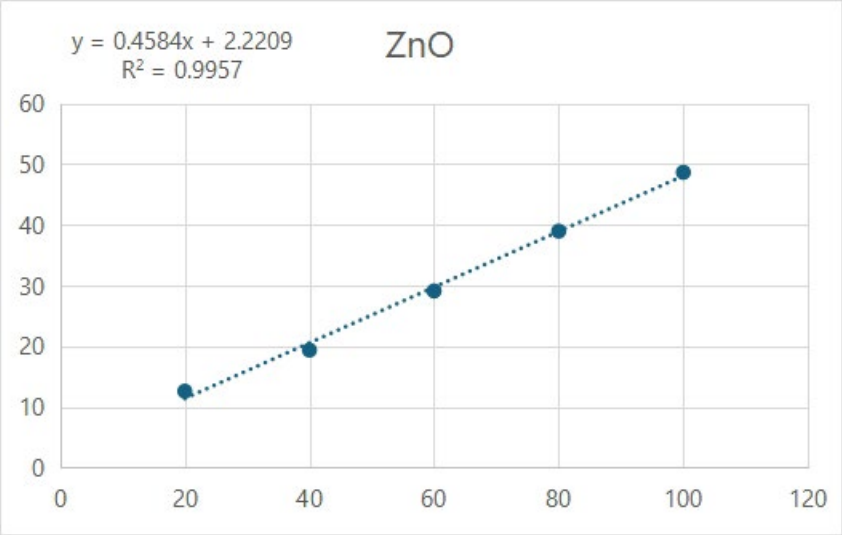

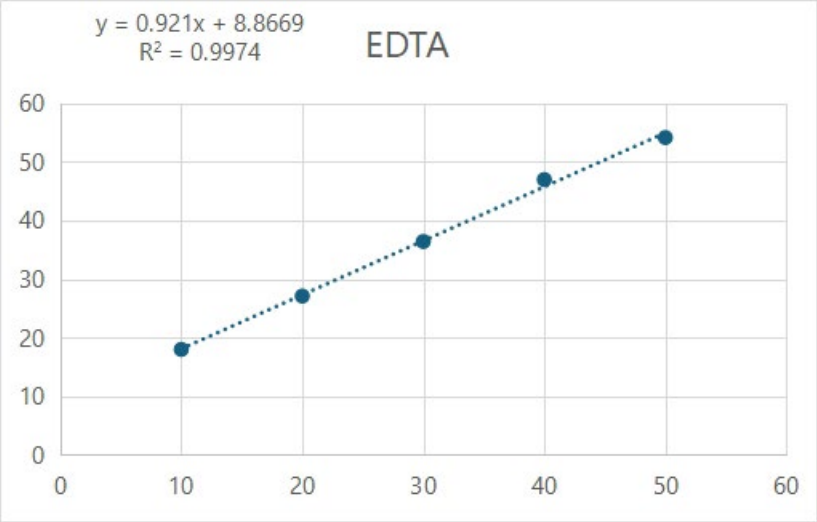

4. Conclusion

In this study, ZnO nanoparticles (ZnO NPs) were effectively synthesized via a green and sustainable approach using germinated *Eleusine coracana* extract as an organic stabilizing and reducing agent. The method was simple, cost-effective, and environmentally friendly. XRD analysis confirmed the ZnO NPs are crystalline, with an average crystallite size of about 28 nm. UV–visible spectroscopy revealed a distinctive absorption peak with a band gap energy of 2.19 eV at 368 nm, confirming nanoparticle formation. TEM analysis revealed predominantly spherical nanoparticles with slight agglomeration and polycrystalline nature, while DLS analysis indicated a typical particle size of 107.3 nm. Significant

antibacterial action against Aspergillus flavus, Pichia anomala, Staphylococcus aureus, Enterococcus faecalis, Escherichia coli, and Pseudomonas aeruginosa was demonstrated by the produced ZnO NPs. The ZnO NPs also demonstrated DPPH IC₂₀ value of 104.23 µg/mL indicates a moderate level of antioxidant activity, whereas negligible ferrous-ion chelating activity was observed. Overall, the results indicate that germinated finger millet extract is an effective biological source for ZnO NP synthesis with promising antimicrobial and antioxidant agent for future applications.

Acknowledgement

The authors are thankful to the Department of Botany and Department of Chemistry, Davangere University, Davangere for providing necessary laboratory facilities to conduct the experiments.

References

1. Gudkov, S. V., Burmistrov, D. E., Serov, D. A., Rebezov, M. B., Semenova, A. A., & Lisitsyn, A. B. (2021). A mini review of antibacterial properties of ZnO nanoparticles. *Frontiers in Physics*, *9*, 641481.
2. Islam, F., Shohag, S., Uddin, M. J., Islam, M. R., Nafady, M. H., Akter, A., ... &Cavalu, S. (2022). Exploring the journey of zinc oxide nanoparticles (ZnO-NPs) toward biomedical applications. *Materials*, *15*(6), 2160.
3. Liu, L., Nian, H., & Lian, T. (2022). Plants and rhizospheric environment: Affected by zinc oxide nanoparticles (ZnO NPs). A review. *Plant Physiology and Biochemistry*, *185*, 91-100.
4. Mukhopadhyay, S. S. (2014). Nanotechnology in agriculture: prospects and constraints. *Nanotechnology, science and applications*, 63-71.
5. Lahiri, D., Nag, M., Ghosh, S., & Ray, R. R. (2021). Green synthesis of nanoparticles and their applications in the area of bioenergy and biofuel production. In *Nanomaterials* (pp. 195-219). Academic Press.
6. Díaz-Álvarez, A. E., &Cadierno, V. (2013). Glycerol: a promising green solvent and reducing agent for metal-catalyzed transfer hydrogenation reactions and nanoparticles formation. *Applied Sciences*, *3*(1), 55-69.
7. Hu, F., Lin, R., Huang, Y., Lai, W., Zheng, H., Huang, H., & Xie, S. (2025). Turning sodium lignosulfonate waste from pulping and papermaking into a green separation agent for energy-efficient biofuel purification. *Chemical Engineering Journal*, *519*, 165563.
8. Chandra, D., Chandra, S., & Sharma, A. K. (2016). Review of Finger millet (Eleusine coracana (L.) Gaertn): A power house of health benefiting nutrients. *Food Science and Human Wellness*, *5*(3), 149-155.
9. Shobana, S., Krishnaswamy, K., Sudha, V., Malleshi, N. G., Anjana, R. M., Palaniappan, L., & Mohan, V. (2013). Finger millet (Ragi, Eleusine coracana L.): a review of its nutritional properties, processing, and plausible health benefits. *Advances in food and nutrition research*, *69*, 1-39.
10. Naveen, P., Mamidi, G., & Priyadarsini, I. (2025). Millet-Mediated Green Synthesis of Zinc Oxide Nanoparticles: Dual Antidiabetic and Antioxidant Mechanisms toward Nano-Nutraceutical Applications.
11. Sharma, V. K., &Marbaniang, D. (2019). Characterization Techniques of Nanoparticles Applied in Drug Delivery Systems. In *Nanotechnology* (pp. 25-56). CRC Press.

12. Chirayil, C. J., Abraham, J., Mishra, R. K., George, S. C., & Thomas, S. (2017). Instrumental techniques for the characterization of nanoparticles. In *Thermal and rheological measurement techniques for nanomaterials characterization* (pp. 1-36). Elsevier.
13. Janaki, A. C., Sailatha, E., & Gunasekaran, S. (2015). Synthesis, characteristics and antimicrobial activity of ZnO nanoparticles. *Spectrochimica Acta Part A: Molecular and Biomolecular Spectroscopy*, *144*, 17-22..
14. Suresh, D., Nethravathi, P. C., Rajanaika, H., Nagabhushana, H., & Sharma, S. C. (2015). Green synthesis of multifunctional zinc oxide (ZnO) nanoparticles using Cassia fistula plant extract and their photodegradative, antioxidant and antibacterial activities. *Materials Science in Semiconductor Processing*, *31*, 446-454.
15. Bayrami, A., Parvinroo, S., Habibi-Yangjeh, A., & Rahim Pouran, S. (2018). Bio-extract-mediated ZnO nanoparticles: microwave-assisted synthesis, characterization and antidiabetic activity evaluation. *Artificial cells, nanomedicine, and biotechnology*, *46*(4), 730-739.
16. Abdelbaky, A. S., Mohamed, A. M., Sharaky, M., Mohamed, N. A., & Diab, Y. M. (2023). Green approach for the synthesis of ZnO nanoparticles using Cymbopogon citratus aqueous leaf extract: characterization and evaluation of their biological activities. *Chemical and Biological Technologies in Agriculture*, *10*(1), 63.
17. Dobrucka, R., &Długaszewska, J. (2016). Biosynthesis and antibacterial activity of ZnO nanoparticles using Trifolium pratense flower extract. *Saudi journal of biological sciences*, *23*(4), 517-523.
18. Ogunyemi, S. O., Abdallah, Y., Zhang, M., Fouad, H., Hong, X., Ibrahim, E., ... & Li, B. (2019). Green synthesis of zinc oxide nanoparticles using different plant extracts and their antibacterial activity against Xanthomonas oryzae pv. oryzae. *Artificial cells, nanomedicine, and biotechnology*, *47*(1), 341-352.
19. Sukri, S. N. A. M., Shameli, K., Wong, M. M. T., Teow, S. Y., Chew, J., & Ismail, N. A. (2019). Cytotoxicity and antibacterial activities of plant-mediated synthesized zinc oxide (ZnO) nanoparticles using Punica granatum (pomegranate) fruit peels extract. *Journal of Molecular Structure*, *1189*, 57-65.
20. Ramesh, M., Anbuvannan, M., &Viruthagiri, G. J. S. A. P. A. M. (2015). Green synthesis of ZnO nanoparticles using Solanum nigrum leaf extract and their antibacterial activity. *Spectrochimica Acta Part A: Molecular and Biomolecular Spectroscopy*, *136*, 864-870.
21. Sundrarajan, M., Ambika, S., & Bharathi, K. (2015). Plant-extract mediated synthesis of ZnO nanoparticles using Pongamia pinnata and their activity against pathogenic bacteria. *Advanced powder technology*, *26*(5), 1294-1299.
22. Ambika, S., &Sundrarajan, M. (2015). Antibacterial behaviour of Vitex negundo extract assisted ZnO nanoparticles against pathogenic bacteria. *Journal of Photochemistry and photobiology B: Biology*, *146*, 52-57.
23. Velsankar, K., Parvathy, G., Sankaranarayanan, K., Mohandoss, S., & Sudhahar, S. (2022). Green synthesis of silver oxide nanoparticles using Panicum miliaceum grains extract for biological applications. *Advanced Powder Technology*, *33*(7), 103645.
24. Bulla, S. S., Bhajantri, R. F., & Chavan, C. (2021). Optical and structural properties of biosynthesized silver nanoparticle encapsulated PVA (Ag–PVA) films. *Journal of Inorganic and Organometallic Polymers and Materials*, *31*(6), 2368-2380.

25. Prashanth, G. K., Prashanth, P. A., Nagabhushana, B. M., Ananda, S., Krishnaiah, G. M., &Sathyananda, H. M. (2015). In vitro antibacterial and cytotoxicity studies of ZnOnanopowders prepared by combustion assisted facile green synthesis. *Karbala International Journal of Modern Science*, *1*(2), 67-77.
26. Choudhary, S., Kumawat, G., Khandelwal, M., Khangarot, R. K., Saharan, V., Nigam, S., & Harish. (2024). Phyco-synthesis of silver nanoparticles by environmentally safe approach and their applications. *Scientific Reports*, *14*(1), 9568.
27. Perez, C. (1990). Antibiotic assay by agar-well diffusion method. *Acta Biol Med Exp*, *15*, 113-115.
28. Dinis, T. C., Madeira, V. M., & Almeida, L. M. (1994). Action of phenolic derivatives (acetaminophen, salicylate, and 5-aminosalicylate) as inhibitors of membrane lipid peroxidation and as peroxyl radical scavengers. *Archives of biochemistry and biophysics*, *315*(1), 161-169.
29. Van Heerden, J. L., & Swanepoel, R. (1997). XRD analysis of ZnO thin films prepared by spray pyrolysis. *Thin Solid Films*, *299*(1-2), 72-77..
30. Bouderbala, I. Y., Guessoum, A., Rabhi, S., Herbadji, A., & Bouras, I. E. (2025). Layer-dependent photocatalytic efficiency of ZnO Thin films: kinetic analysis, structural insights and optical bandgap characterization using absorption spectrum fitting, Tauc's plot, and Cody models. *Journal of Materials Science: Materials in Electronics*, *36*(27), 1782.
31. Jubu, P. R., Obaseki, O. S., Yam, F. K., Stephen, S. M., Avaa, A. A., McAsule, A. A., ... &Otor, D. A. (2023). Influence of the secondary absorption and the vertical axis scale of the Tauc's plot on optical bandgap energy. *Journal of Optics*, *52*(3), 1426-1435.
32. Talam, S., Karumuri, S. R., & Gunnam, N. (2012). Synthesis, characterization, and spectroscopic properties of ZnO nanoparticles. *International Scholarly Research Notices*, *2012*(1), 372505.
33. Mohan, A. C., &Renjanadevi, B. J. P. T. (2016). Preparation of zinc oxide nanoparticles and its characterization using scanning electron microscopy (SEM) and X-ray diffraction (XRD). *Procedia Technology*, *24*, 761-766.
34. Hasnidawani, J. N., Azlina, H. N., Norita, H., Bonnia, N. N., Ratim, S., & Ali, E. S. (2016). Synthesis of ZnO nanostructures using sol-gel method. *Procedia chemistry*, *19*, 211-216.
35. Salavati-Niasari, M., Davar, F., & Khansari, A. (2011). Nanosphericals and nanobundles of ZnO: Synthesis and characterization. *Journal of Alloys and Compounds*, *509*(1), 61-65.
36. Chen, C., Liu, J., Liu, P., & Yu, B. (2011). Investigation of photocatalytic degradation of methyl orange by using nano-sized ZnO catalysts. *Advances in Chemical Engineering and Science*, *1*(01), 9-14.
37. Díez-Pascual, A. M. (2018). Antibacterial activity of nanomaterials. *Nanomaterials*, *8*(6), 359.
38. Slavin, Y. N., Asnis, J., Häfeli, U. O., & Bach, H. (2017). Metal nanoparticles: understanding the mechanisms behind antibacterial activity. *Journal of nanobiotechnology*, *15*(1), 65.